Article

A Luminescent Nanocellulose Platform: from Controlled Graft Block Copolymerization to Bio-marker Sensing

Julien R.G. Navarro, Stefan Wennmalm, Jamie Godfrey, Magnus Breiholtz, and Ulrica M Edlund

Biomacromolecules, **Just Accepted Manuscript** • DOI: 10.1021/acs.biomac.5b01716 • Publication Date (Web): 20 Jan 2016

A Luminescent Nanocellulose Platform: from Controlled Graft Block Copolymerization to Bio-marker Sensing

Julien R.G. Navarro[†], *Stefan Wennmalm*[‡], *Jamie Godfrey*[†], *Magnus Breitholtz*[§]

*and Ulrica Edlund**[†]

[†]Fiber and Polymer Technology, Royal Institute of Technology (KTH), Teknikringen 56, SE-100 44, Stockholm, Sweden

[‡]Science for Life Laboratory, Department of Applied Physics, KTH-Royal Institute of Technology, SE-171 65 Solna, Sweden

[§]Department of Environmental Science and Analytical Chemistry, Stockholm University, SE-114 18 Stockholm, Sweden

ABSTRACT

A strategy is devised for the conversion of cellulose nanofibrils (CNF) into fluorescently labelled probes involving the synthesis of CNF-based macroinitiators that initiate radical polymerization of methyl acrylate and acrylic acid N-hydroxysuccinimide ester producing a graft block copolymer modified CNF. Finally, a luminescent probe (Lucifer yellow derivative) was labelled onto the modified CNF through an amidation reaction. The surface modification steps were verified with solid-state ^{13}C nuclear magnetic resonance (NMR), and Fourier transform infrared spectroscopy. Fluorescence Correlation Spectroscopy (FCS) confirmed the successful labelling of the CNF, the CNF have a hydrodynamic radius of about 700 nm with an average number of dye molecules per fibril of at least 6600. The modified CNF was also imaged with confocal laser scanning microscopy. Luminescent CNF proved to be viable bio-markers and allow for fluorescence-based optical detection of CNF uptake and distribution in organisms such as crustaceans. The luminescent CNF were exposed to live juvenile daphnids and microscopy analysis revealed the presence of the luminescent CNF all over D. magna's alimentary canal tissues without any toxicity effect leading to the death of the specimen.

KEYWORDS: Cellulose nanofibrils, controlled radical polymerization, grafting, luminescent cellulose, fluorescent correlation spectroscopy, bio-marker

INTRODUCTION

Nanocellulose, fibril nanoparticles of sub-micrometer thickness from cellulose, have attracted considerable attention over the last decades as they are biodegradable, renewable and recyclable with strong potential for a range of applications, from composites to drug delivery.[1] Nanocellulose can be extracted from various sources (cotton, woods or algae) and under different forms: Cellulose nanofibrils (CNF) assimilated to long wires are composed of amorphous and crystalline domains, while cellulose nanocrystals (CNC) are described as small rods, where the amorphous regions are removed through acid hydrolysis.[2–4] The nanocellulose structure provides good mechanical and thermal properties, and thereby could be used as a powerful reinforcing filler for composite films[1,5]. However, surface modification remained necessary for their further use in specific applications in order to obtain a sufficient interaction of the nanocellulose with the polymer matrix. Thanks to the abundance of hydroxyl groups on the nanocellulose surface,[6] several synthetic approaches have been exploited such as click-chemistry,[7,8] esterification,[9,10] etherification,[11] silylation,[12] and oxidation.[13] In most cases, the substitution degree, and hence polymer matrix compatibility was relatively low, and nanocellulose dispersion in various organic solvents remained difficult. Therefore, there is a real need of a surface modification approach that produce chemically modified CNF which yield stable CNF suspensions in numerous organic solvents and allow for facile handling and subsequent chemical functionalization. Controlled ring opening polymerization (ROP) has been used to graft and polymerize ε-caprolactone onto nanocellulose, yielding a stable suspension in toluene.[14–16] Moreover, ROP modification allowed for processing of a nanocellulose-based nanocomposite with a significant improvement of the initial, undoped, mechanical properties. Majoinen *et al.*[17] demonstrated that it was possible to obtain stable nanocellulose suspension, either in aqueous or organic solvents, through surface

initiated controlled radical polymerization. Yi *et al.*[18] modified cellulose nanocrystals through the controlled polymerization of N,N-Dimethylaminoethyl methacrylate and obtained a thermally sensitive chiral nematic phase change in suspension.

Recently, it has been shown that polysaccharides can be efficiently converted to brominated or chlorinated macro-initiators for Cu(0)-mediated controlled radical polymerization through partial substitution of their hydroxyl groups.[19–23] Cu(0)-mediated radical polymerization, introduced as Single Electron Transfer Living Radical Polymerization (SET-LRP) by Percec and co-workers[24–27], proved to be an efficient technique as it can be performed in water and under non-inert conditions with full control on the molecular weight.[28–32] SET-LRP is described to occur *via* an electron transfer from the Cu(0) catalyst to an alkyl halide initiator and the dormant propagating chain end.[25] Cu(0)-mediated controlled radical polymerization has been demonstrated to be viable for a wide range of vinyl monomers.[33] In view of the above, Cu(0)-mediated controlled radical polymerization offers a strong potential applied to polysaccharide functionalization and offer new opportunities to customize nanocellulose chemistry for specific applications and desired property profiles.

The labelling of nanocellulose with fluorescent probes is of great interest as bio-markers and in sensor applications.[34–39] Within the standard fluorescence spectroscopy and microscopy, Mahmoud *et al.*[40] monitored the *in situ* cellular uptake of fluorescently labelled cellulose nanocrystals and evaluated its cytotoxicity. Colombo *et al.*[41] modified cellulose nanocrystals with Alexa Fluor 633 and studied their toxicity through intravenous injection in living organisms. In both studies, nanocellulose proved to be an efficient material platform for biomedical applications.

Among the rich library of commercially available dyes, Lucifer Yellow has the advantage of being water soluble, stable against photo-bleaching and useful for biological applications.[42–46] So far, to study the photophysical properties of a dye at the single molecule level, and to verify the correct labelling of the dye on an entity, fluorescence correlation spectroscopy (FCS) has proven to be one of the most potent techniques.[47,48] FCS detects fluorescently labelled particles diffusing through a femtoliter detection focus, and provides information about the diffusion coefficient and the particle concentration (picomolar to micromolar range).[49,50] From the diffusion coefficient the hydrodynamic radius can be derived which indicates the particle size. In single colour mode, FCS can differentiate the detected fluorescence signal of a free dye from a signal of a dye labelled larger objects such as proteins,[51] and nanoparticles.[52] During the last 20 years FCS and related fluctuation techniques have developed into a widely used and commercially available tool to analyse biomolecular interactions and fluctuations, in solution or in living cells.[53–55]

In terms of water ecology and ecotoxicology studies, the cladoceran Daphnia magna (D. magna), a small freshwater shellfish, has been used for several years now as a standardized test organism.[56] Daphnia magna are filter feeders, ingesting algae into their mouth through a self-produced water current. These animals are stable even if exposed to different feeding sources and various stresses.[57,58] By exposing them to fungi, viruses or bacteria, the stress-induced response is detectable.[59,60] One remarkable feature of the D. magna resides in their transparent shell, which makes them an ideal candidate for microscopy studies. Teplova *et al*.[61] used different dyes to separate and image the intoxication-death step in the D. magna body. By feeding D. magna with luminescent objects, it remained possible to study the ecotoxicity of a material.

Our aim was to develop luminescent CNF by controlled radical polymerization of block copolymer grafts from purposely synthesized NFC-based macroinitiators. The first polymer block comprises methyl acrylate to enhance the stability of the suspension, suppressing fibril-fibril interactions, whilst the second block is composed of acrylic acid N-hydroxysuccinimide ester, in order to introduce functional anchoring sites that are modified with a luminescent dye. FCS and confocal scanning laser microscopy enabled determination of the photophysical properties in suspension and at the molecular scale of the resulting fluorescently tagged CNF. We finally exposed the fluorescently modified CNF to living juvenile daphnids to explore the bio-marker potential.

EXPERIMENTAL SECTION

Materials

1,1'-Carbonyldiimidazole (CDI), 2-Bromo-2-methylpropionic acid 98%, imidazole ≥ 99%, methyl acrylate 99% and acrylic acid N-hydroxysuccinimide ester ≥ 90% were purchased from Sigma-Aldrich. Dimethyl sulfoxide (DMSO, ≥ 99%) was purchased from Merck. Lucifer Yellow cadaverine was purchased from Interchim. Copper wire (diameter 0.812 mm) was purchased from Fisher. For the production of cellulose nanofibrils a bleached never-dried softwood sulphite dissolving pulp (Domsjö mill, Domsjö Fabriker AB, Sweden) was used. A mono-component endoglucanase (FiberCare® R, Novozymes, Denmark) was used as received. Milli-Q water was used for the solvent exchange procedure.

Extraction of cellulose nanofibrils (CNF) from wood pulp

The CNF was prepared by a combined refining and enzymatic pre-treatment procedure as described by Pääkkö *et al.*[62] prior to homogenization in a Microfluidizer M-110EH (Microfluidics Corp., USA). No biocide was added after the pre-treatment. The homogenization was carried out at about 2% w/w concentration with repeated passes through fixed Z-shaped chamber pairs connected in series. First, the fibre slurry was passed three times through a chamber set with dimensions of 400 and 200 μm followed by five passes through a chamber set with dimensions of 200 and 100 μm at 1700 bar. The total charge density of the CNF was determined to be 40 μeq/g by conductometric titration[63] of the unhomogenized pulp. Scanning Elecron Microscopy micrographs of the lyophilized CNF are shown in Figure S1 (Supporting information).

Solvent exchange procedure

7 g of CNF (2.06 % w/w) were suspended in 50 mL of water and subsequently stirred for 5 h. The suspension was then sonicated for 5 min and again stirred for 3 h. The suspension was finally distributed (10 mL) into several centrifugation tubes and DMSO (30 mL) was added. The tubes was then centrifuged (4000 RPM, 20 min), the supernatants removed and replaced with fresh DMSO. The centrifugation operation was repeated 4 times.

CNF-based macroinitiator synthesis

2-Bromo-2-methylpropionic acid (2 g, 12 mmol) was dissolved in 30 mL DMSO and mixed with CDI (1.95 g, 12 mmol) at room temperature for 1 h. Subsequently, the temperature was raised to 55°C and a suspension composed of CNF (5 g, 1 % w/w) and imidazole (1.5 g, 22 mmol) in 50

mL of DMSO was slowly added. The reaction proceeded for 16 h. Finally, the modified CNF were purified by centrifugation (4 000 RPM / 20 min). The supernatants were discarded and replaced with DMSO. The purification steps were repeated 8 times. The modified CNF was characterized by FTIR spectroscopy and solid-state MAS ^{13}C NMR.

Tris[2-(dimethylamino)ethyl]amine (Me_6-TREN) synthesis

Me_6-TREN was synthesized according to literature.[64] Briefly, tris(2-aminoethyl)amine (15 g, 0.1 mol) was added dropwise to a solution composed of formaldehyde (160 mL) and formic acid (160 mL) previously cooled to 0°C. After 1 h stirring, the solution was allowed to warm to room temperature and subsequently refluxed for 16 h. The solution was concentrated by rotary evaporation, washed with a saturated solution of NaOH and the product was extracted with dichloromethane. The solvent was finally removed and the slightly yellow liquid was dried overnight under vacuum before purification by vacuum distillation.

Polymerization reactions

The CNF-based macroinitiator was suspended in DMSO (10 mL), followed by the addition of 3 g of monomer, either methyl acrylate (MA) or acrylic acid N-hydroxysuccinimide ester (NAS). A piece of copper wire (diameter=0.812 mm, length=6.25 cm) was added and the suspension was degassed *via* nitrogen sparging for 10 minutes and the temperature was raised to 40°C. The Me_6TREN ligand was added and the reaction was allowed to proceed for 16h, under a nitrogen atmosphere. The modified CNF were purified through several centrifugation steps (4 000 RPM /

20 min). The different reactants were used with the ratio $[M]_0/[I]_0/[L]_0$ of 200/1/0.2 for the SET-LRP of MA and $[M]_0/[I]_0/[L]_0$ = 30/1/0.2 for NAS. The modified CNF batches were characterized by FTIR spectroscopy and solid-state MAS ^{13}C NMR.

Fluorescent labelling with Lucifer Yellow cadaverine

The block copolymer modified CNF (2 g, 1 % w/w) was suspended in DMSO (8 mL) before addition of 2 mL DMSO solution composed of Lucifer Yellow cadaverine (20 mg, 37 µmol) and triethylamine (22 µL), and stirred at 40°C for 48 h. The luminescent CNF was purified through several centrifugation steps (4 000 RPM / 20 min), and the purification step was repeated until no fluorescent signal was detected in the supernatant. The luminescent CNF was characterized by fluorescence spectroscopy, fluorescence correlation spectroscopy (FCS) and confocal scanning laser microscopy.

CNF uptake in Daphnia magna.

Daphnia magna is a freshwater crustacean and an established model species in ecotoxicological, ecological and evolutionary studies. The animals used in this study originate from the test strain ‘‘Klon 5’’, the State office for nature, environment, and customer protection North-Rhine Westfalia, Bonn, Germany; originally from the Federal Environment Agency, Berlin, Germany). Daphnids were cultured in M7 medium[65,66] in groups of ~25 females in 2 L containers and fed a

mixture of the green algae *Pseudokirchneriella subcapitata* and *Scenedesmus subspicatus* three times a week.

Characterization

Infrared spectroscopy was performed using a PerkinElmer Spectrum 2000 spectrometer, equipped with an attenuated total reflection (ATR) accessory. Measurements were normally performed by accumulating 64 scans in the spectral region of 4000–550 cm^{-1} with a spectral resolution of

4 cm^{-1}.

Fluorescence spectra were obtained using a Varian Cary Eclipse Fluorescence spectrophotometer. Single nanoparticle fluorescence visualization was performed using an inverted Zeiss Axiovert Observer.Z1 microscope equipped with a LSM5 exciter. The sample was visualized with a 63x/1.4 NA oil-immersion objective lens, excited with a diode laser (405 nm), together with a beam splitter (HFT 405/488/543/633) and a long-pass filter (LP 530).

Fluorescence microscopy was used to identify the uptake and presence of CNF in the guts of the daphnids. Pictures were taken on live juvenile daphnids (age 24-48 old) sampled from the culture and immediately exposed to 1 g/L CNF for 3 hours. The microscope-camera-setup consisted of a Canon EOS 5d Mark III camera (Canon Inc, Tokyo, Japan) mounted via a camera tube (model: DD20DMT, Diagnostics Instruments Inc, Sterling Heights, USA) to a Leitz DMRBE microscope (Leica microsystems GmbH, Wetzlar, Germany).

Field-emission Scanning electron microscopy (FE-SEM) imaging was performed with a Hitachi S-4800 field emission scanning electron microscope, operating at 1 kV. Samples were mounted on carbon tape-coated stubs and sputter coated with a 12 nm thick layer of Pt/Pd using a Cressington 20HR sputter coater.

All ^{13}C NMR experiments were performed with a Bruker 500 Avance III HD spectrometer at Larmor frequencies of 125 MHz and 500 MHz for ^{13}C and ^{1}H, respectively. The samples were packed in 4 mm zirconia rotors and spun at 8 kHz. Ramped cross-polarization (CP) ^{13}C MAS NMR spectra were recorded with a ^{13}C nutation frequency of 50 kHz and contact time 1.5 ms. High-power ^{1}H decoupling was achieved by the TPPM technique using a nutation frequency of 80 kHz. 4096 signal transients were accumulated with relaxation delays from 3 to 15 s, depending on relaxation time estimated for each sample. Signal apodization by an 30 Hz Lorentzian broadening was applied before Fourier transformation and ^{13}C chemical shifts are quoted relative to neat tetramethylsilane (TMS).

FCS measurements were performed on an FCS-equipped Zeiss 780 confocal microscope (Zeiss, Jena, Germany). The sample was excited by a 405 nm laser line (300 μW) focused through a C-Apochromat 40X/1.2 NA water-immersed objective via a dichroic mirror. The fluorescence was detected by the same objective and was spectrally divided and detected by a 32 channel GaAsP detector after passage through a pinhole in the image plane. The size of the confocal detection volume was estimated by measurements on the dye Lucifer Yellow, which was assumed to have a diffusion coefficient of about 400 $\mu m^2/s$ in in water and thereby a diffusion coefficient of about 200 $\mu m^2/s$ in DMSO. This yielded a detection volume of 0.2 fL. FCS analysis was performed using the Zen 2012 software (Zeiss, Jena, Germany) as well as in house written functions using Origin 9.1 (Originlab Corporation, USA). The autocorrelation function in an FCS experiment is calculated as:

$$G(\tau) = \frac{<F(t)\cdot F(t+\tau)>}{<F(t)>^2} = \frac{<\delta F(t)\cdot \delta F(t+\tau)>}{<F(t)>^2} + 1$$

Here F is the detected fluorescence intensity, δF is the deviation from the mean fluorescence intensity at a certain time point, ($\delta F(\tau) = F(\tau) - \langle I \rangle$), and brackets denote mean value.

For a sample containing particles of uniform size, and where translational diffusion is the only process giving rise to fluorescence fluctuations, the autocorrelation function in an FCS measurement is fitted to:

$$G(\tau)=\frac{1}{N}\frac{1}{(1+\frac{\tau}{\tau_D})}\frac{1}{(1+\frac{\omega^2\tau}{z^2\tau_D})^{1/2}}+1$$

Where N is the mean number of particles in the detection volume, τD is the diffusion time of particles through the detection volume, and ω and z denote the distances in the radial and axial dimensions respectively, at which the average detected fluorescence intensity has dropped to e-2 of its peak value.

RESULTS AND DISCUSSION

To produce a (multi)functional platform, bio-marker or sensor, cellulose nanofibrils (CNF) were chemically modified through an esterification reaction and two consecutive Cu(0)-mediated controlled radical polymerizations to further exploit the build-up of block copolymer grafts and the labelling of specific entities. In contrast to the so-called TEMPO-oxidized CNF,[13] where the native cellulose is converted/processed to individual fibrils through the introduction of surface charges which induce an electrostatic repulsion between the fibrils, our CNF source was composed of an abundant numbers of hydroxyl groups on the surface, enhancing the possibility of an inter-fibril interaction. The growth of the first polymer block aims to suppress this tendency of fibril-to-fibril aggregation, yielding a stable CNF suspension over the time. The second polymer block will allow introducing reactive functionality on to the CNF surface, producing a highly reactive CNF platform toward amine-based entities. Finally, the block copolymers

modified CNF was labelled with a water-soluble luminescent probe through an amidation reaction.

Firstly, CNF-based macroinitiators were successfully prepared via an esterification reaction between 2-Bromo-2-methylpropionic acid and the hydroxyl group of the nanocellulose backbone, yielding–C(CH3)2-Br pendant groups on the surface (Scheme 1).

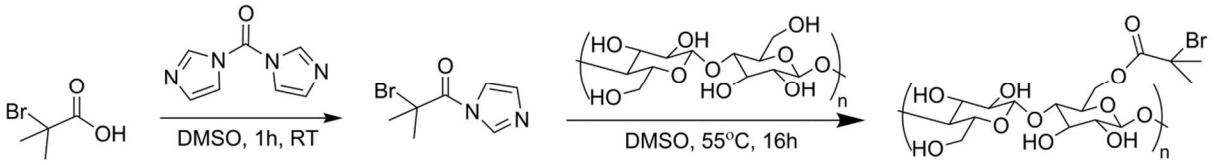

Scheme 1. Synthetic pathway for the preparation of CNF-based macroinitiators.

Next, we explored the ability of the CNF-based macroinitiator to initiate Cu(0)-mediated controlled radical polymerizations of methyl acrylate (MA) and acrylic acid N-hydroxysuccinimide ester (NAS) monomers, respectively (Scheme 2). The polymerization of MA, initiated by the modified CNF, was conducted run in the presence of Cu(0) and a tetradendate tertiary amine ligand (Me_6TREN) in DMSO (Scheme 2a). After several purification steps, the graft polymer modified CNF initiated the second SET-LRP of the NAS monomer, yielding a reactive block copolymer modified CNF. In these two polymerization steps, the monomer feeds were set to achieve a higher degree of polymerization of the first block (factor: 6.6). Finally, the Lucifer yellow cadaverine was labelled onto the modified CNF through an amidation reaction (Scheme 2b).

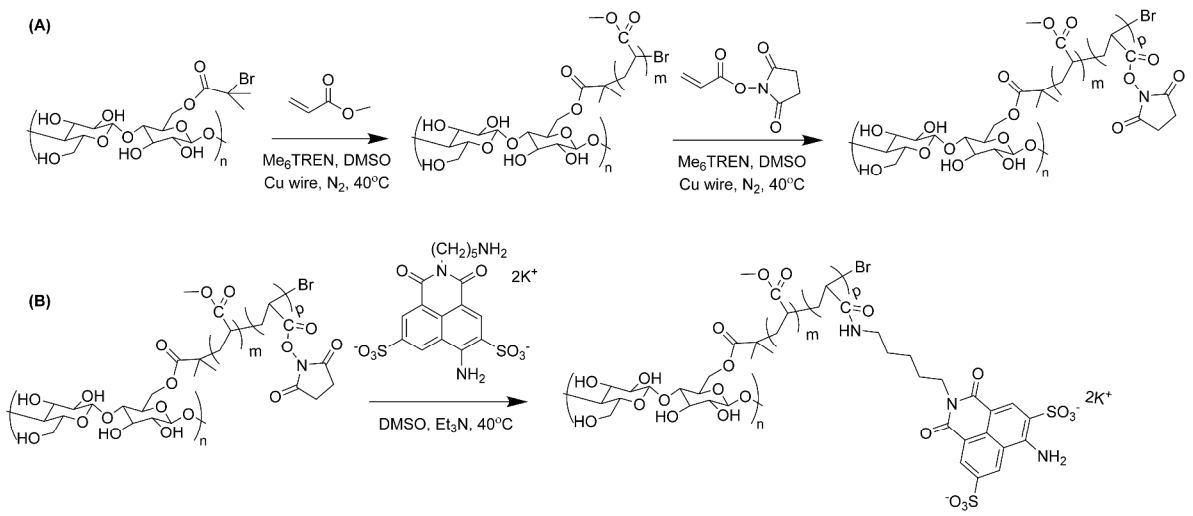

Scheme 2. Synthetic pathway for the labelling of fluorescent probes onto surface modified CNF: (a) Synthesis of a block copolymer onto CNF-based macroinitiators through SET-LRP with methyl acrylate and acrylic acid N-hydroxysuccinimide ester. (b) Fluorescent labelling of the block copolymer-modified CNF with the Lucifer yellow cadaverine by amidation.

The structures of the different chemically modified CNF were verified by ATR-FTIR and are compared in Figure 1. Unmodified CNF (Figure 1a) shows the characteristic absorption bands located at 3320 cm^{-1} (O-H), 2950 and 2895 cm^{-1} (C-H), 1430 cm^{-1} (C-H) and 1161 cm^{-1} (C-O-C). In addition to these absorption bands, the CNF-based macroinitiator (Figure 1b) shows an additional band located at 1736 cm^{-1}, attributed to the carbonyl group. Unfortunately, this additional absorption band is not intense, due to a relatively low substitution degree of the 2-bromo-2-methylpropionic acid onto the CNF. Nevertheless, the FTIR spectra of the polymer-modified CNF (Figure 1c) shows strong additional absorption bands located at 2954 cm^{-1} (C-H), 1727 cm^{-1} (C=O), 1437 cm^{-1} (C-H), 1159 cm^{-1} (C-O-C) indicating the expected grafting of PMA. With the addition of the second monomer (NAS), the spectra of the block copolymer modified CNF did not show any new absorption bands. The (initial) absorption bands of the NAS

monomer were located at 1821 cm^{-1}, 1775 cm^{-1} and 1711 cm^{-1}, attributed to the succinimide group, and 1200 cm^{-1} (C-O, ester) overlapped with the absorption bands of the first polymer block modified-CNF bands. Moreover, the carbonyl band intensity (or ratio if compared to the OH band) did not increase since the precursor ratio was different for the two blocks (factor: 6.6). Indeed, the second chain block will have a shorter degree of polymerization if compared to the first block. The different FTIR spectra indicate that the surface modifications of the CNF through an esterification reaction and subsequent graft polymerization were successful.

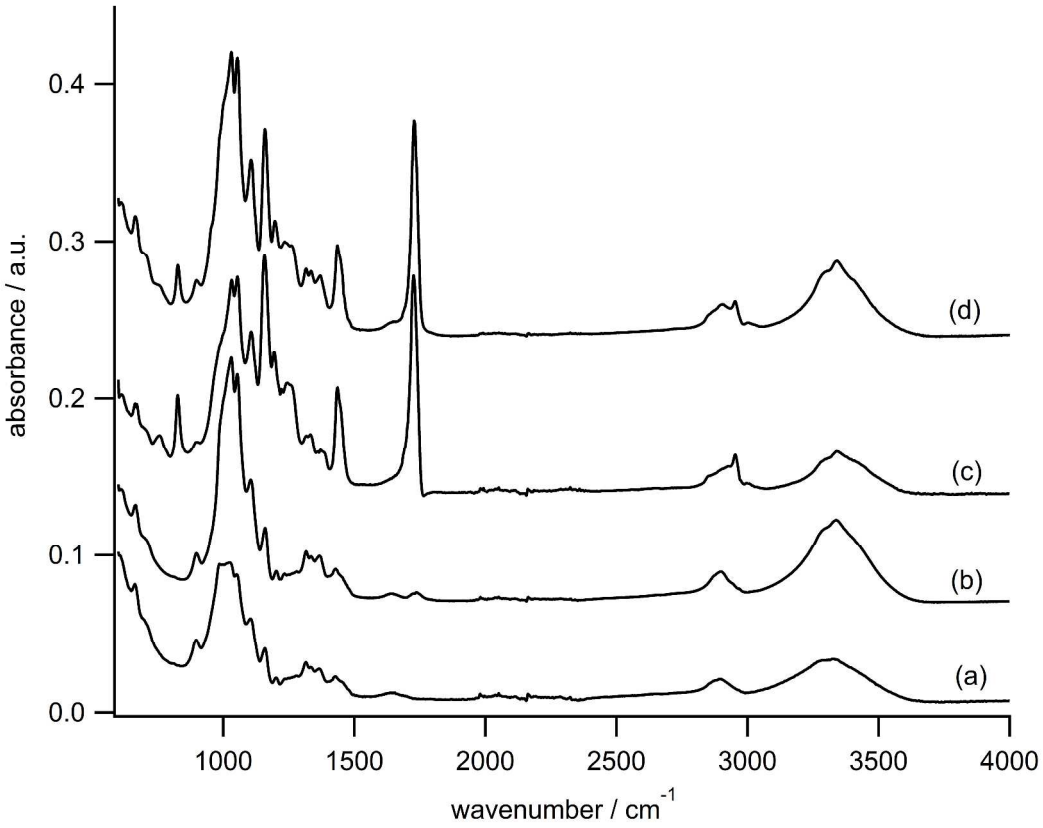

Figure 1. FTIR spectra of (a) unmodified CNF, (b) CNF-based macroinitiators, (c) Poly(MA)-grafted CNF and (d) Poly(MA-block-NAS)-grafted CNF.

CPMAS ^{13}C spectra of unmodified cellulose nanofibrils, CNF-based macroinitiator, and poly(MA-block-NAS)-grafted CNF, as well as the corresponding chemical structures are shown in Figure 2, with the various chemical shifts provided at the top of each spectrum. The spectrum of the initial, unmodified, CNF showed the characteristic bands of cellulose, with bands located at 84 ppm (C4) and 62 ppm (C6) for the surface carbon sites, at 89 (C4) and 66 ppm (C6) for the carbon inside the crystalline region. These peak positions agreed with previous reports.[67–69] The CNF-based macroinitiator spectrum (Figure 2b) includes a new carbonyl bond signal (C7, 169 ppm), which has low intensity compared to the integration of the peaks from the initial cellulose, from which a substitution degree of 2 % was estimated. This observation confirmed the relatively low substitution degree of the 2-bromo-2-methylpropionate onto the CNF, in agreement with the previous observations made with FTIR. The poly(MA-block-NAS)-grafted CNF spectrum (Figure 2c), on the other hand, shows the appearance of new intense peaks characteristic of the MA-block-NAS: the ^{13}C NMR peak at 175 ppm is attributed to the sites C12, C16 and C17 (carbonyl bond); the band located at 52 ppm corresponds to the methyl group (C13) and the methylene in β-position of the carbonyl group (C10 and C14), whereas the bands located between 41 and 36 ppm are attributed to the sites C11, C15 and C18. The integration of the NMR peaks revealed a ratio of 0.9 of the poly(MA-block-NAS)-grafted polymer to the signal of the initial cellulose. Unfortunately, it was not possible to isolate the carbonyl bonds signals from the MA block and the NAS block, and thus estimate the polymerization degree of each block.

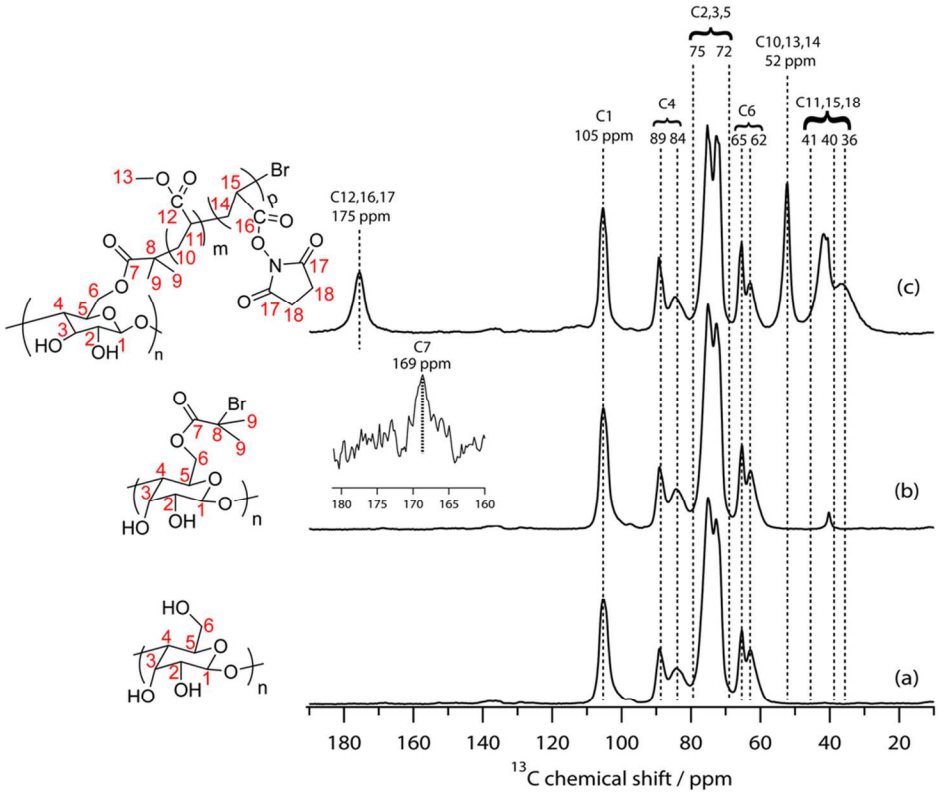

Figure 2. Solid state ^{13}C NMR spectra at 500 mHz and chemical structures of a) CNF, b) CNF-based macroinitiator, and (c) Poly(MA-block-NAS)-grafted CNF. The spinning side bands are localized at 138.8, 136.2, 11.8 and 9.2 ppm.

UV-visible and fluorescence spectra of Lucifer yellow and the Lucifer yellow labelled CNF suspended in DMSO are shown in Figure 3. For a better comparison the absorption and emission spectrum were rescaled with respect to the maximum intensity. The Lucifer yellow is characterized by absorption and emission bands localized at 435 nm and 514 nm, respectively. The spectra confirmed that tethering of the free Lucifer yellow to the block copolymer-modified CNF did not affect the position of the absorption-emission bands.

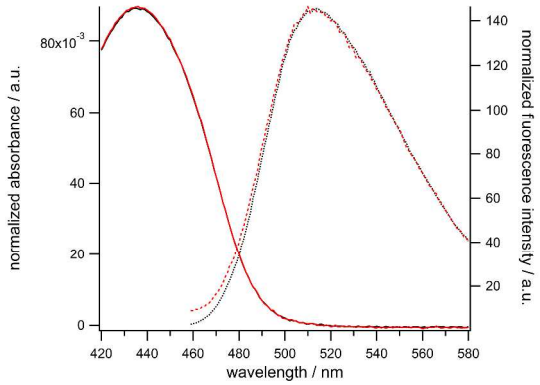

Figure 3. Normalized UV-Visible (solid line) and fluorescence spectra (dashed line) of Lucifer yellow (black) and Lucifer yellow labelled onto CNF (red).

One of the most appropriate techniques for probing the photophysical properties of a dye at the single molecule level is fluorescence correlation spectroscopy (FCS),[47,48] since it is possible to detect the intensity fluctuation of a single chromophore passing through the focal point. Through this approach, a small volume (< 1 μL) of highly diluted chromophore solution (pM) is excited through a focused laser beam passing by a microscope objective. The subsequent fluorescence is detected *via* a confocal pinhole and monitored through a single-photon detector. Each time a chromophore diffuses through the observation volume a fluorescence signal is generated, and the fluctuations thus generated are analyzed by the automatically calculated correlation function. This technique will provide information on the photodynamics of the dye (blinking, photobleaching), as well as the concentration and diffusion time of the luminescent species (i.e. small molecules or large objects will have fast or slow diffusion times, respectively) in the focal volume.[52,70]

In our experiment, the unlabelled Lucifer Yellow (LY), i.e. the free dye, and the Lucifer yellow labelled CNF (LY-CNF) were studied with FCS. The fluorescence correlation curves are shown

in Figure 4 and the results are summarized in Table 1. The free dye curve (Figure 4, top) is composed only of fast diffusing molecules in the focal volume (τ_{diff}=45 μs). In the case of the dye-labelled CNF (Figure 4, bottom), the fluorescence signal is drastically different and is only composed of slowly diffusing species, i.e. large objects. The diffusion time of the luminescent fibrils was estimated to be 500 ms. This corresponds to a diffusion coefficient of fluorescent CNF of D_{CNF}≈0.018 $\mu m^2/s$, approximately 11 000 times smaller than that of LY, D_{LY}≈200 $\mu m^2/s$. In the most highly concentrated samples of CNF, FCS yielded a concentration of 0.35 nM on average.

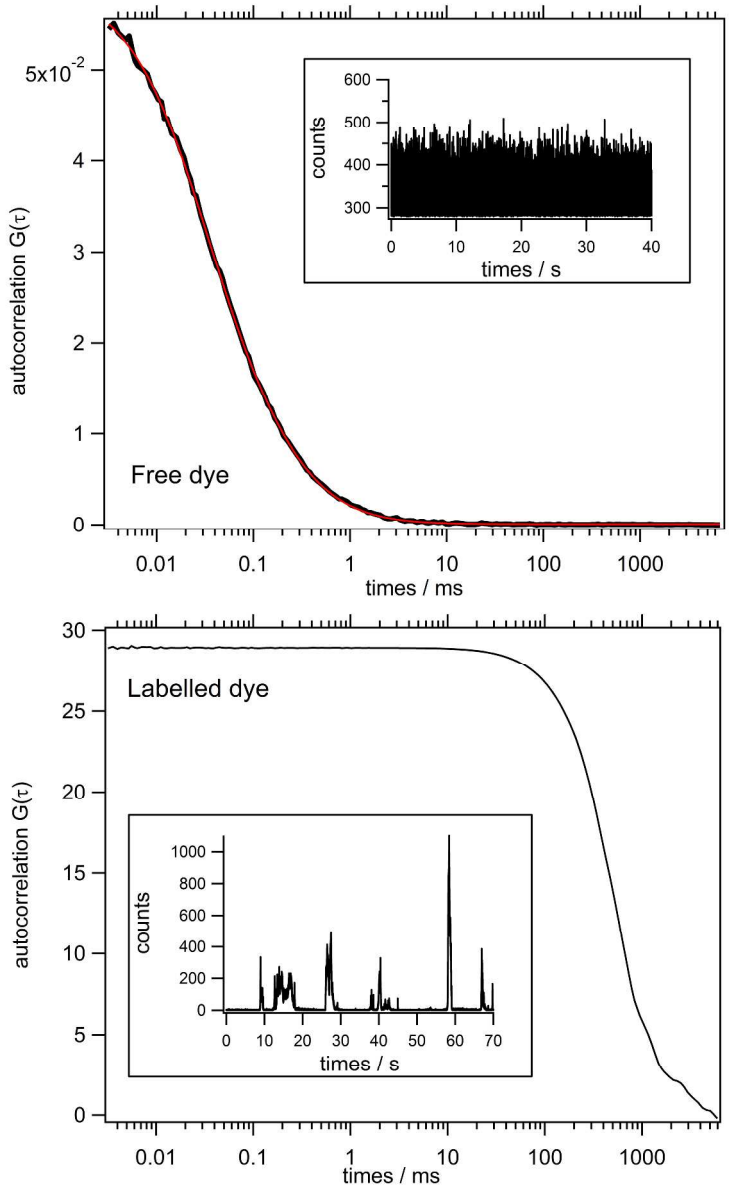

Figure 4. Fluorescence correlation curves of Lucifer yellow (LY), unlabelled dye (top) and Lucifer yellow-modified CNF (bottom). Both samples were recorded in DMSO.

It is worth noting that the amplitude of the two autocorrelation curves is highly different. The curve amplitude is inversely dependent of the average number of fluorescent molecules diffusing in the focal volume. As such, as the autocorrelation amplitude increased, the number of observed

chromophores decreased. From the estimated concentration and the fluorescence count-rate the brightness of the dye can be calculated. The brightness of LY was 18.7 kHz per molecule when excited at 300 μW, whereas the brightness of the LY- CNF was 247 kHz per molecule (i.e. per fibril) when excited at 0.6 μW. Taking the measured difference in brightness as well as the difference in laser power into account, the CNF fibrils were approximately 6600 times brighter than individual LY dye molecules, and accordingly each CNF should contain at least 6600 LY dye molecules.

As a control experiment, and to ensure that nonspecific binding between the free dyes with the CNF was not possible, a separate measurement was performed by simply mixing the LY with the chemically modified CNF-based macroinitiators. That measurement yielded a diffusion time of 45 μs, which corresponds to the diffusion time of the free dye. Thus, nonspecific binding between the free dyes and the CNF was not observed, thus we conclude that the luminescent signal stems from LY covalently bound to the CNF.

Table 1. Summary of the results obtained by FCS for the LY free dye and labelled onto the modified CNF in DMSO.

Samples	τ_{diff} / μs	Brightness / kHz	Brightness of CNF/ Brightness of LY
LY	45	18.7	-------
LY_CNF	5 x10^5	247[a]	6600
Physical blend	45	18.7	0

[a]The brightness of the LY-labelled CNF was 247 kHz per fibril.

In FCS the diffusion coefficient D is usually given by the measured diffusion time (τ_D) from the equation $\tau_D=\omega^2/4D$, and from D the hydrodynamic radius R_h of the particles can be obtained from the Stokes-Einstein equation. However in the current situation, the analyzed CNF[62,71] are not spherical particle within the nanometer scale range but instead object with a size larger than the detection focus. Thus, the measured τ_D must be interpreted differently in order not to overestimate the R_h value.

Based on the results from Wu *et al*.[72], we extrapolate our result, and with changing the solvent viscosity, a diffusion time of 500 ms corresponds to a hydrodynamic radius of 700 nm (Figure 5).

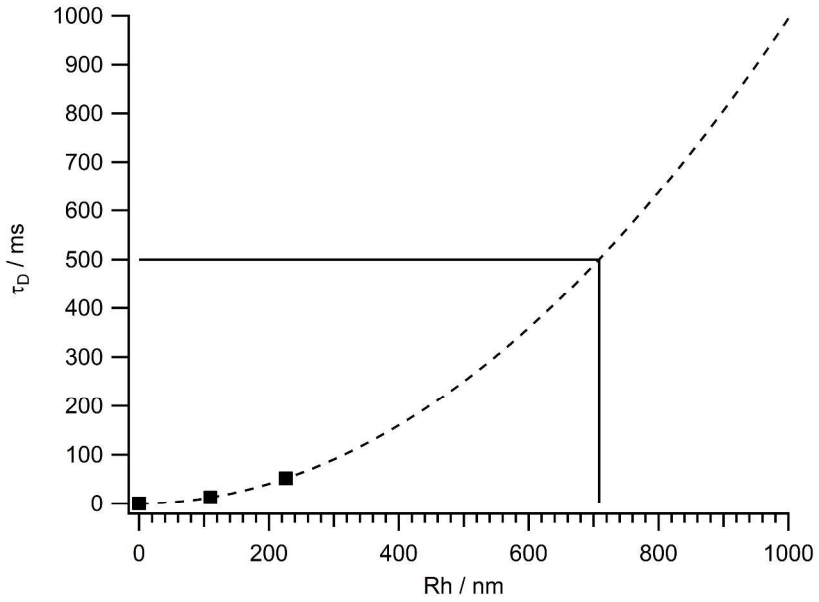

Figure 5. Estimation of the hydrodynamic radius R_h of the CNF. Two particle sizes with their diffusion time, plus the origo, were converted from Wu *et al.*[72], adjusted for the viscosity of DMSO, and fitted with a second order polynomial for extrapolation.

As concluded above, the average hydrodynamic radius of CNF was 700 nm and the average fluorescence brightness per fibril corresponds to that of 6600 LY fluorophores. The hydrodynamic radius corresponds to a spherical particle volume of about 1.5 fL, while the FCS detection volume is about 0.19 fL. In other words, the part of the CNF which is inside the FCS detection volume gives rise to a fluorescence signal corresponding to 6600 LY fluorophores, but a spherically shaped CNF would be about eight times larger than the FCS detection. Accordingly, if the fibrils are spherically shaped then each fibril is labelled about 8 times more than the 6600 LY detected (50 000LY unit/CNF). If instead the fibrils are rod-shaped, they are most likely aggregated, since a rod-shaped CNF of 5 nm diameter would not be able to accommodate enough LY fluorophores inside the FCS detection volume without causing significant fluorescence quenching.

Confocal laser scanning microscopy was used to image the LY labelled on the block copolymer-modified CNF. The fluorescence images were obtained with a 405 nm excitation wavelength, with a beam splitter (HFT 405/488/543/633) and a long-pass filter (LP 530). The resulting images (fluorescence and combined overlay fluorescence-bright-field images) were obtained with two different magnifications and are shown in Figure 6. For clearer visualization, the dyes were spotted in blue. Luminescent spots were only observed along the CNF, which confirmed the absence of unlabelled dye in the suspension. Moreover, the fluorescent spots were homogeneously distributed onto the CNF.

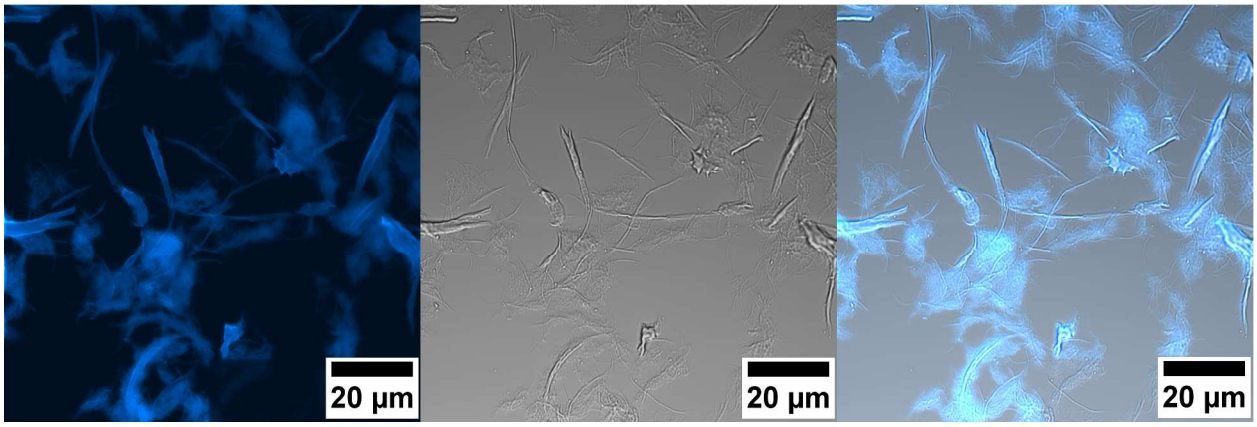

Figure 6. Confocal scanning laser microscopy imaging of LY labelled on the block copolymer-modified CNF. (Left) Fluorescence image obtained with an excitation wavelength of 405 nm, (middle) bright-field image (right) combined overlay fluorescence-bright-field images.

In the previous sections we have shown that the chromophore-labelled CNFs exhibit the desired fluorescence, allowing precise imaging of the fibrils by confocal laser scanning microscopy. As such it may serve as a potential bio-marker that allow for the fluorescence-based optical detection of CNF uptake and distribution in living organisms. For this purpose, we choose the *Daphnia magna.* Daphnids were cultured in M7 medium[65,66] in groups of ~25 females and fed a mixture of the green algae *Pseudokirchneriella subcapitata* and *Scenedesmus subspicatus* three times a week. The live juvenile daphnids were then exposed to the LY-CNF (1g/L) for 3 h. During this period, no dead species were observed. The experiment was repeated 5 times to ensure a good reproducibility. Thanks to their transparent shell, fluorescence microscopy was used to identify the uptake and presence of CNF in the guts of the daphnids (Figure 7). The bright field images revealed the presence of green algae in the D. magna's alimentary canal

tissues, while the fluorescence images revealed the presence of the luminescent CNF throughout the alimentary canal (Figure 7, top). No fluorescence signal was detected on the control specimen (Figure 7, bottom). Thus, the D. magna ingested the luminescent CNF, which then dissipates within the algae in the guts of the daphnids, demonstrating the non-toxicity of our material for the viability of the species. In case of toxic fluorescent material,[61] the fluorescence emission would have changed due to the lack of transmembrane potential. These results highlight the non-toxicity of the modified CNF and as a new kind of nanomaterial based on wood, it remains highly important to prove their biocompatibility for their future use in bio-applications.

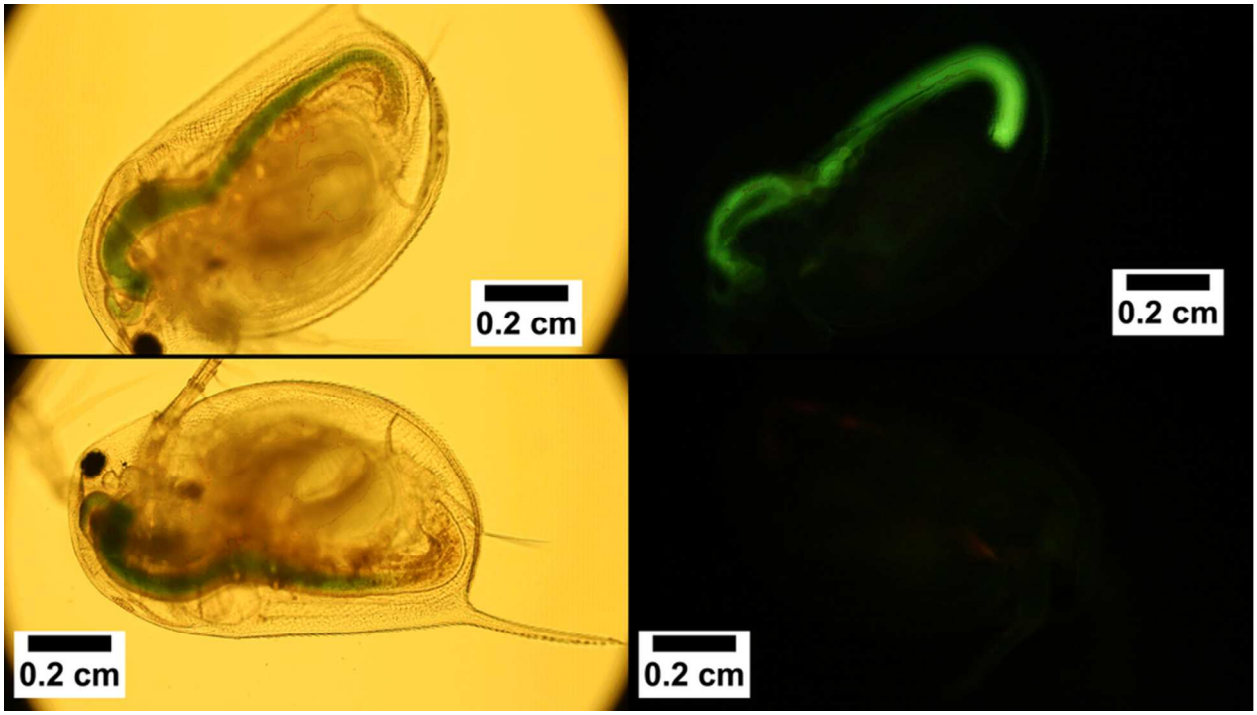

Figure 7. Bright field (left) and fluorescence (right) images of Daphnia magna in (bottom) control experiment and (top) exposed to LY-CNF.

CONCLUSIONS

A strategy toward luminescent nanocellulose is devised based on the principle of controlled radical graft copolymerization and photophysically probed on the molecular scale by FCS. CNF were first converted to CNF-based macroinitiators able to initiate Cu(0)-mediated controlled radical polymerization, producing block methyl acrylate-co-acrylic acid N-hydroxysuccinimide ester grafted from the CNF backbones. A luminescent probe (Lucifer yellow derivative) was then coupled to the modified CNF. FCS probing confirmed that CNF was successfully labelled by LY fluorophores. For ecotoxicity purpose, the luminescent CNF were exposed to live juvenile daphnids. After 3 hours, the specimens were subjected to microscopy analysis, revealing the presence of the luminescent CNF throughout D. magna's alimentary canal tissues with no toxicity leading to the death of the specimen. Luminescent CNF were proved to be viable bio-markers and allow for fluorescence-based optical detection of CNF uptake and distribution in organisms such as crustaceans.

ASSOCIATED CONTENT

Supporting Information. Figure S1. SEM picture of the unmodified CNF**.** This material is available free of charge *via* the Internet at http://pubs.acs.org.

AUTHOR INFORMATION

Corresponding Author

***Email:** edlund@polymer.kth.se

Author Contributions

The manuscript was written through contributions of all authors. All authors have given approval to the final version of the manuscript.

Funding Sources

The Swedish research council Formas (project no 2014-151).

Notes

The authors declare no competing financial interest.

ACKNOWLEDGMENT

The authors thank Formas (project number 2014-151) for financial support. We also thank E. Ålander at Innventia AB for the preparation of nanocellulose.

REFERENCES

(1) Kalia, S.; Dufresne, A.; Cherian, B. M.; Kaith, B. S.; Avérous, L.; Njuguna, J.; Nassiopoulos, E. *Int. J. Polym. Sci.* **2011**, *2011*, 1–35.

(2) Moon, R. J.; Martini, A.; Nairn, J.; Simonsen, J.; Youngblood, J. *Chem. Soc. Rev.* **2011**, *40*, 3941–3994.

(3) Eichhorn, S. J.; Dufresne, A.; Aranguren, M.; Marcovich, N. E.; Capadona, J. R.; Rowan, S. J.; Weder, C.; Thielemans, W.; Roman, M.; Renneckar, S.; Gindl, W.; Veigel, S.; Keckes, J.; Yano, H.; Abe, K.; Nogi, M.; Nakagaito, A. N.; Mangalam, A.; Simonsen, J.; Benight, A. S.; Bismarck, A.; Berglund, L. A.; Peijs, T. *J. Mater. Sci.* **2010**, *45*, 1–33.

(4) Klemm, D.; Kramer, F.; Moritz, S.; Lindström, T.; Ankerfors, M.; Gray, D.; Dorris, A. *Angew. Chem. Int. Ed* **2011**, *50*, 5438–5466.

(5) Salas, C.; Nypelö, T.; Rodriguez-Abreu, C.; Carrillo, C.; Rojas, O. J. *Curr. Opin. Colloid Interface Sci.* **2014**, *19*, 383–396.

(6) Habibi, Y. *Chem. Soc. Rev.* **2014**, *43*, 1519–1542.

(7) Koschella, A.; Hartlieb, M.; Heinze, T. *Carbohydr. Polym.* **2011**, *86*, 154–161.

(8) Filpponen, I.; Argyropoulos, D. S. *Biomacromolecules* **2010**, *11*, 1060–1066.

(9) Nielsen, L. J.; Eyley, S.; Thielemans, W.; Aylott, J. W. *Chem. Comm.* **2010**, *46*, 8929–8931.

(10) Sassi, J.-F.; Chanzy, H. *Cellulose* **1995**, *2*, 111–127.

(11) Eyholzer, C.; Bordeanu, N.; Lopez-Suevos, F.; Rentsch, D.; Zimmermann, T.; Oksman, K. *Cellulose* **2010**, *17*, 19–30.

(12) Goussé, C.; Chanzy, H.; Cerrada, M. L.; Fleury, E. *Polymer (Guildf).* **2004**, *45*, 1569–1575.

(13) Isogai, A.; Saito, T.; Fukuzumi, H. *Nanoscale* **2011**, *3*, 71–85.

(14) Habibi, Y.; Goffin, A.-L.; Schiltz, N.; Duquesne, E.; Dubois, P.; Dufresne, A. *J. Mater. Chem.* **2008**, *18*, 5002.

(15) Lönnberg, H.; Larsson, K.; Lindström, T.; Hult, A.; Malmström, E. *ACS Appl. Mater. Interfaces* **2011**, *3*, 1426–1433.

(16) Carlmark, A.; Larsson, E.; Malmström, E. *Eur. Polym. J.* **2012**, *48*, 1646–1659.

(17) Majoinen, J.; Walther, A.; McKee, J. R.; Kontturi, E.; Aseyev, V.; Malho, J. M.; Ruokolainen, J.; Ikkala, O. *Biomacromolecules* **2011**, *12*, 2997–3006.

(18) Yi, J.; Xu, Q.; Zhang, X.; Zhang, H. *Cellulose* **2009**, *16*, 989–997.

(19) Edlund, U.; Rodriguez-Emmenegger, C.; Brynda, E.; Albersson, A.-C. *Polym. Chem.* **2012**, *3*, 2920.

(20) Edlund, U.; Albertsson, A.-C. *J. Polym. Sci., Part A Polym. Chem.* **2011**, *49*, 4139–4145.

(21) Dax, D.; Xu, C.; Långvik, O.; Hemming, J.; Backman, P.; Willför, S. *J. Polym. Sci. Part A Polym. Chem.* **2013**, *51*, 5100–5110.

(22) Voepel, J.; Edlund, U.; Albertsson, A. C. *J. Polym. Sci. Part A Polym. Chem.* **2011**, *49*, 2366–2372.

(23) Zoppe, J. O.; Habibi, Y.; Rojas, O. J.; Venditti, R. a.; Johansson, L.-S.; Efimenko, K.; Österberg, M.; Laine, J. *Biomacromolecules* **2010**, *11*, 2683–2691.

(24) Percec, V.; Guliashvili, T.; Ladislaw, J. S.; Wistrand, A.; Stjerndahl, A.; Sienkowska, M. J.; Monteiro, M. J.; Sahoo, S. *J. Am. Chem. Soc.* **2006**, *128*, 14156–14165.

(25) Rosen, B. M.; Percec, V. *Chem. Rev.* **2009**, *109*, 5069–5119.

(26) Zhang, N.; Samanta, S. R.; Rosen, B. M.; Percec, V. *Chem. Rev.* **2014**, *114*, 5848–5958.

(27) Nguyen, N. H.; Levere, M. E.; Kulis, J.; Monteiro, M. J.; Percec, V. *Macromolecules* **2012**, *45*, 4606–4622.

(28) Edlund, U.; Albertsson, A. C. *J. Polym. Sci. Part A Polym. Chem.* **2012**, *50*, 2650–2658.

(29) Zhang, Q.; Wilson, P.; Li, Z.; McHale, R.; Godfrey, J.; Anastasaki, A.; Waldron, C.; Haddleton, D. M. *J. Am. Chem. Soc.* **2013**, *135*, 7355–7363.

(30) Nguyen, N. H.; Kulis, J.; Sun, H.-J.; Jia, Z.; van Beusekom, B.; Levere, M. E.; Wilson, D. A.; Monteiro, M. J.; Percec, V. *Polym. Chem.* **2013**, *4*, 144–155.

(31) Samanta, S. R.; Nikolaou, V.; Keller, S.; Monteiro, M. J.; Wilson, D. A.; Haddleton, D.

M.; Percec, V. *Polym. Chem.* **2015**, 2084–2097.

(32) Aksakal, R.; Resmini, M.; Becer, C. R. *Polym. Chem.* **2016**, *7*, 171–175.

(33) Anastasaki, A.; Nikolaou, V.; Nurumbetov, G.; Wilson, P.; Kempe, K.; Quinn, J. F.; Davis, T. P.; Whittaker, M. R.; Haddleton, D. M. *Chem. Rev.* **2015**, 150730144649001.

(34) Edwards, J. V.; Prevost, N.; Sethumadhavan, K.; Ullah, A.; Condon, B. *Cellulose* **2013**, *20*, 1223–1235.

(35) Schyrr, B.; Pasche, S.; Voirin, G.; Weder, C.; Simon, Y. C.; Foster, E. J. *ACS Appl. Mater. Interfaces* **2014**, *6*, 12674–12683.

(36) Navarro, J. R. G.; Bergström, L. *RSC Adv.* **2014**, *4*, 60757–60761.

(37) Navarro, J. R. G.; Conzatti, G.; Yu, Y.; Fall, A. B.; Mathew, R.; Edén, M.; Bergström, L. *Biomacromolecules* **2015**, *16*, 1293–1300.

(38) Morales-Narváez, E.; Golmohammadi, H.; Naghdi, T.; Yousefi, H.; Kostiv, U.; Horák, D.; Pourreza, N.; Merkoçi, A. *ACS Nano* **2015**, *9*, 7296–7305.

(39) Zhou, D.; Zou, H.; Liu, M.; Zhang, K.; Sheng, Y.; Cui, J.; Zhang, H.; Yang, B. *ACS Appl. Mater. Interfaces* **2015**, *7*, 15830–15839.

(40) Mahmoud, K. A.; Mena, J. A.; Male, K. B.; Hrapovic, S.; Kamen, A.; Luong, J. H. T. *ACS Appl. Mater. Interfaces* **2010**, *2*, 2924–2932.

(41) Colombo, L.; Zoia, L.; Violatto, M. B.; Previdi, S.; Talamini, L.; Sitia, L.; Nicotra, F.; Orlandi, M.; Salmona, M.; Recordati, C.; Bigini, P.; La Ferla, B. *Biomacromolecules* **2015**, *16*, 2862–2871.

(42) Furstenberg, A.; Vauthey, E. *Photochem. Photobiol. Sci.* **2005**, *4*, 260–267.

(43) Stewart, W. W. *Nature* **1981**, *292*, 17–21.

(44) Navarro, J. R. G.; Lerouge, F.; Cepraga, C.; Micouin, G.; Favier, A.; Chateau, D.; Charreyre, M.-T.; Lanoë, P.-H.; Monnereau, C.; Chaput, F.; Marotte, S.; Leverrier, Y.; Marvel, J.; Kamada, K.; Andraud, C.; Baldeck, P. L.; Parola, S. *Biomaterials* **2013**, *34*, 8344–8351.

(45) Pantoja, S.; Lee, C.; Marecek, J. F.; Palenik, B. P. *Anal. Biochem.* **1993**, *211*, 210–218.

(46) Hanani, M. *J. Cell. Mol. Med.* **2012**, *16*, 22–31.

(47) Elson, E. L. *Biophys. J.* **2011**, *101*, 2855–2870.

(48) Thompson, N. L.; Lieto, A. M.; Allen, N. W. *Curr. Opin. Struct. Biol.* **2002**, *12*, 634–641.

(49) Magde, D.; Elson, E.; Webb, W. W. *Phys. Rev. Lett.* **1972**, *29*, 705–708.

(50) Rigler, R.; Mets, U.; Widengren, J.; Kask, P. *Eur. Biophys. J.* **1993**, *22*, 169–175.

(51) Langowski, J. *Methods Cell Biol.* **2008**, *85*, 471–484.

(52) Navarro, J. R. G.; Plugge, M.; Loumaigne, M.; Sanchez-Gonzalez, A.; Mennucci, B.; Débarre, A.; Brouwer, A. M.; Werts, M. H. V. *Photochem. Photobiol. Sci.* **2010**, *9*, 1042–1054.

(53) Schwille, P.; Meyer-Almes, F. J.; Rigler, R. *Biophys. J.* **1997**, *72*, 1878–1886.

(54) Chen, Y.; Müller, J. D.; So, P. T. C.; Gratton, E. *Biophys. J.* **1999**, *77*, 553–567.

(55) Kask, P.; Palo, K.; Ullmann, D.; Gall, K. *Proc. Natl. Acad. Sci. U. S. A.* **1999**, *96*, 13756–13761.

(56) Stollewerk, A. *J. Biol.* **2010**, *9*, 21.

(57) Freese, H. M.; Schink, B. *Microb. Ecol.* **2011**, *62*, 882–894.

(58) Gorokhova, E.; Rivetti, C.; Furuhagen, S.; Edlund, A.; Ek, K.; Breitholtz, M. *Environ. Sci. Technol.* **2015**, *49*, 5779–5787.

(59) Karasov, W. H.; Martínez del Rio, C.; Caviedes-Vidal, E. *Annu. Rev. Physiol.* **2011**, *73*, 69–93.

(60) Harris, J. *Microb. Ecol.* **1993**, *25*, 195–231.

(61) Teplova, V. V.; Andreeva-Kovalevskaya, Z. I.; Sineva, E. V.; Solonin, A. S. *Environ. Toxicol. Chem.* **2010**, *29*, 1345–1348.

(62) Pääkko, M.; Ankerfors, M.; Kosonen, H.; Nykänen, a.; Ahola, S.; Österberg, M.; Ruokolainen, J.; Laine, J.; Larsson, P. T.; Ikkala, O.; Lindström, T. *Biomacromolecules* **2007**, *8*, 1934–1941.

(63) Katz, K.; Beatson, R. P.; Scallan, A. M. *Sven. Papperstidning* **1984**, *87*, R48–R53.

(64) Opsteen, J. A.; Van Hest, J. C. M. *J. Polym. Sci. Pol. Chem.* **2007**, *45*, 2913–2924.

(65) Oecd. *Test No. 202: Daphnia sp. Acute Immobilisation Test*; OECD Guidelines for the Testing of Chemicals, Section 2; OECD Publishing, 2004.

(66) Oecd. *Test No. 211: Daphnia magna Reproduction Test*; OECD Guidelines for the Testing of Chemicals, Section 2; OECD Publishing, 2008.

(67) VanderHart, D. L.; Atalla, R. H. *Macromolecules* **1984**, *17*, 1465–1472.

(68) Isogai, A.; Usuda, M.; Kato, T.; Uryu, T.; Atalla, R. H. *Macromolecules* **1989**, *22*, 3168–3172.

(69) Kono, H.; Yunoki, S.; Shikano, T.; Fujiwara, M.; Erata, T.; Takai, M. *J. Am. Chem. Soc.* **2002**, *124*, 7506–7511.

(70) Loumaigne, M.; Praho, R.; Nutarelli, D.; Werts, M. H. V; Debarre, A. *Phys. Chem. Chem. Phys.* **2010**, *12*, 11004–11014.

(71) Henriksson, M.; Henriksson, G.; Berglund, L. A.; Lindström, T. *Eur. Polym. J.* **2007**, *43*, 3434–3441.

(72) Wu, B.; Chen, Y.; Müller, J. D. *Biophys. J.* **2008**, *94*, 2800–2808.

Table of Contents Graphic

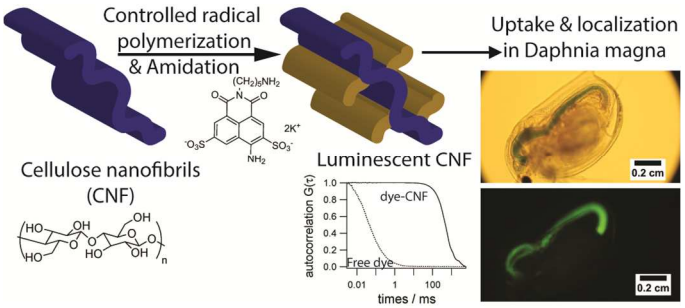
Controlled radical
polymerization
& Amidation
Uptake & localization
in Daphnia magna
Cellulose nanofibrils
(CNF)
Luminescent CNF
dye-CNF
Free dye
autocorrelation G(τ)
times / ms
0.2 cm
0.2 cm

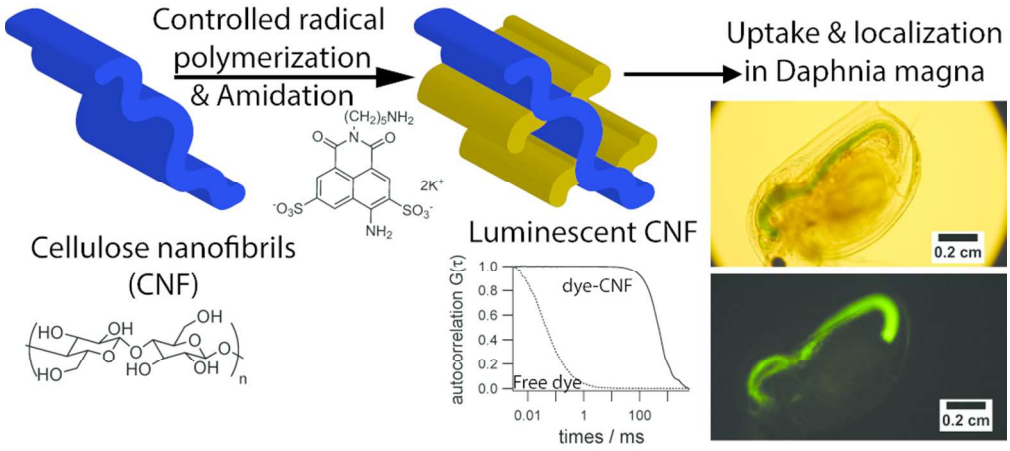

Table of Content graphic
89x40mm (300 x 300 DPI)

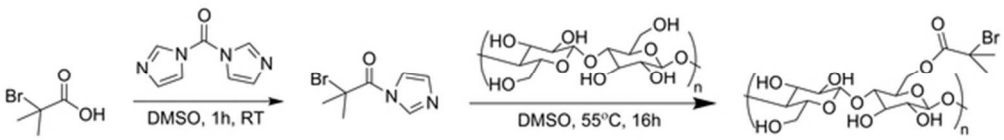

Scheme 1. Synthetic pathway for the preparation of CNF-based macroinitiators.
27x3mm (600 x 600 DPI)

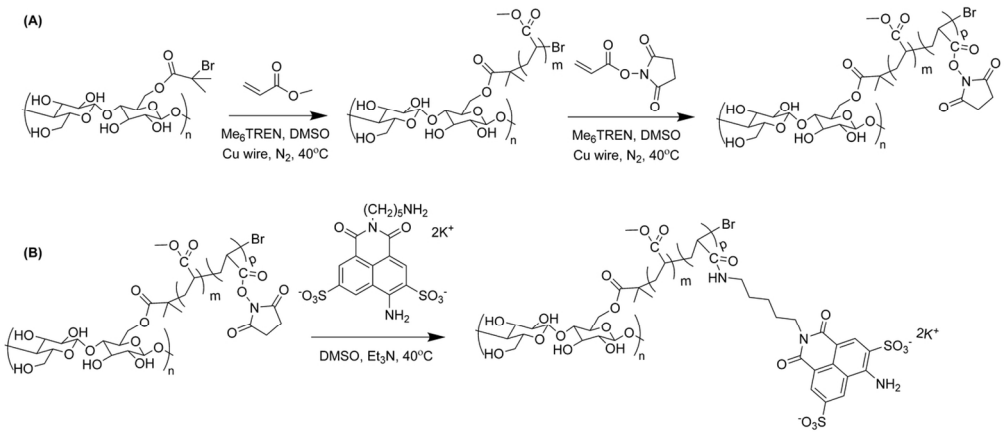

Scheme 2. Synthetic pathway for the labelling of fluorescent probes onto surface modified CNF: (a) Synthesis of a block copolymer onto CNF-based macroinitiators through SET-LRP with methyl acrylate and acrylic acid N-hydroxysuccinimide ester. (b) Fluorescent labelling of the block copolymer-modified CNF with the Lucifer yellow cadaverine by amidation.
60x25mm (600 x 600 DPI)

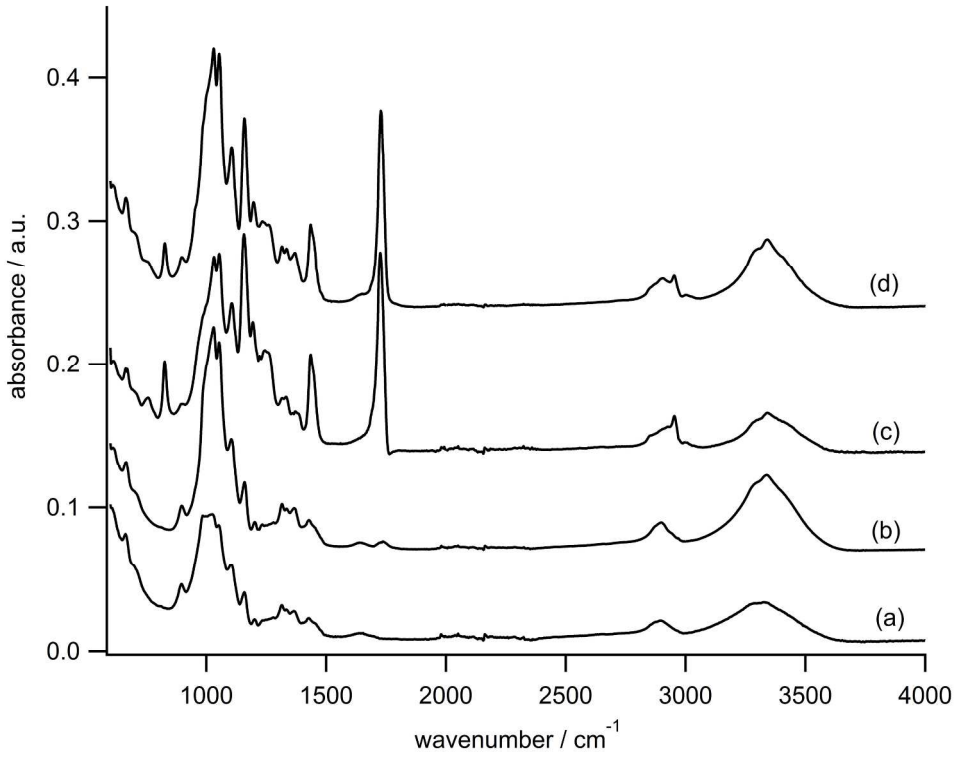

Figure 1. FTIR spectra of (a) unmodified CNF, (b) CNF-based macroinitiators, (c) Poly(MA)-grafted CNF and (d) Poly(MA-block-NAS)-grafted CNF.
115x91mm (600 x 600 DPI)

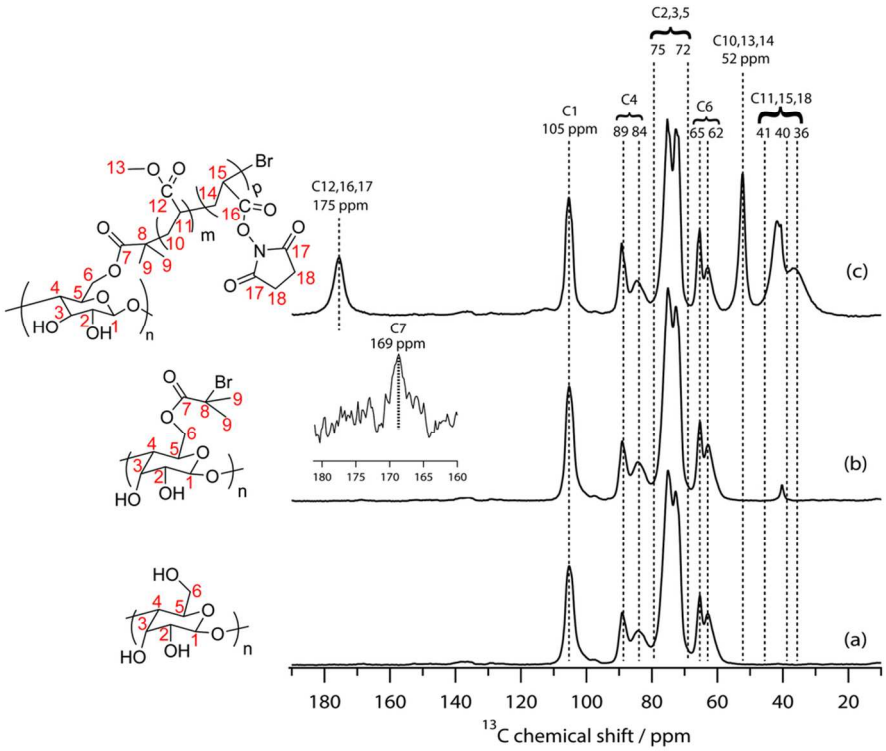

Figure 2. Solid state NMR spectra at 500 mHz and chemical structures of a) CNF, b) CNF-based macroinitiator, and (c) Poly(MA-block-NAS)-grafted CNF. The spinning side bands are marked localized at 138.8, 136.2, 11.8 and 9.2 ppm.

101x75mm (300 x 300 DPI)

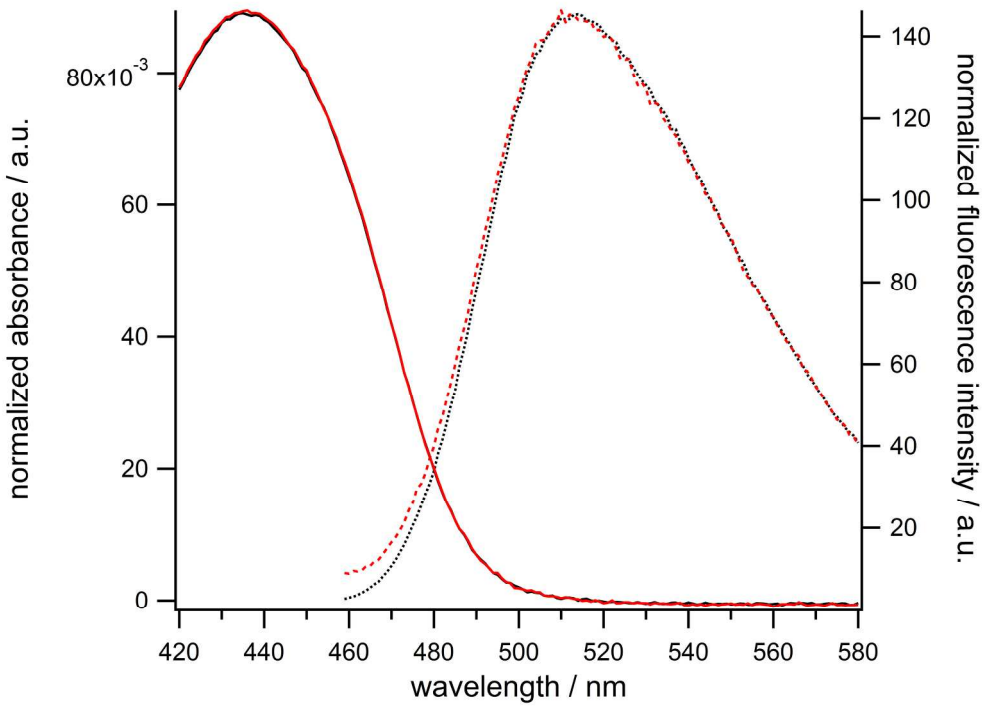

Figure 3. Normalized UV-Visible (solid line) and fluorescence spectra (dashed line) of Lucifer yellow (black) and Lucifer yellow labelled onto CNF (red).
105x78mm (600 x 600 DPI)

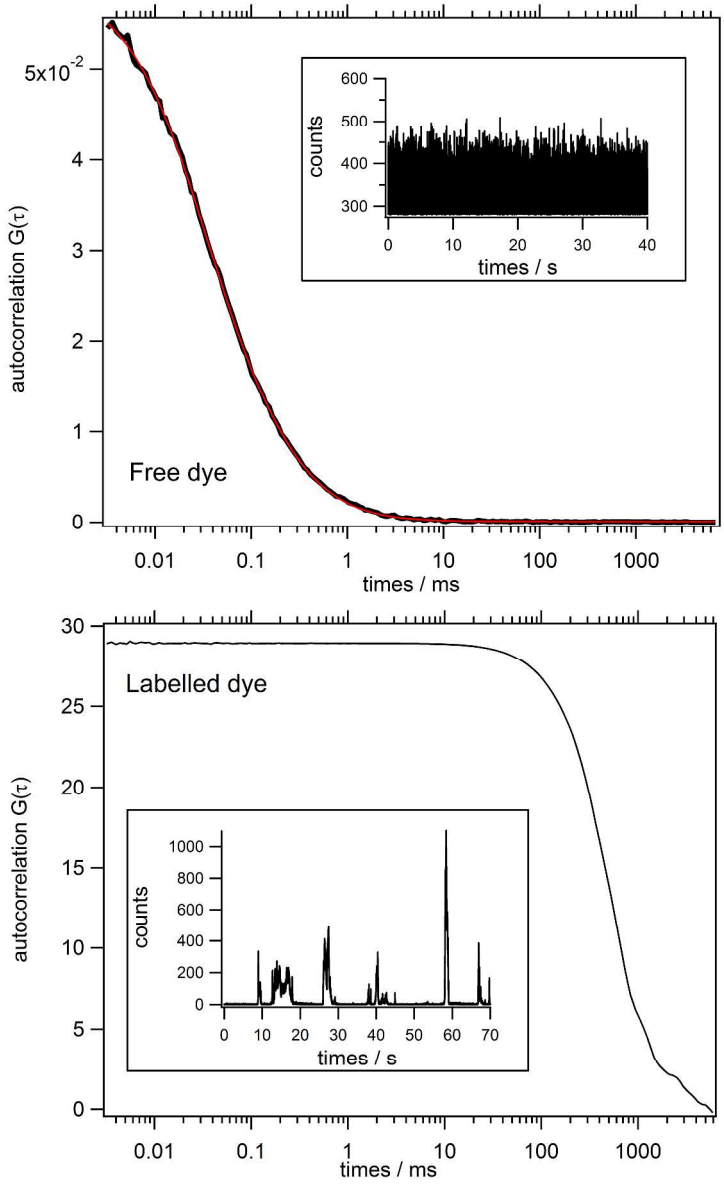

Figure 4. Fluorescence correlation curves of Lucifer yellow (LY), unlabelled dye (top) and Lucifer yellow-modified CNF (bottom). Both samples were recorded in DMSO.
238x359mm (600 x 600 DPI)

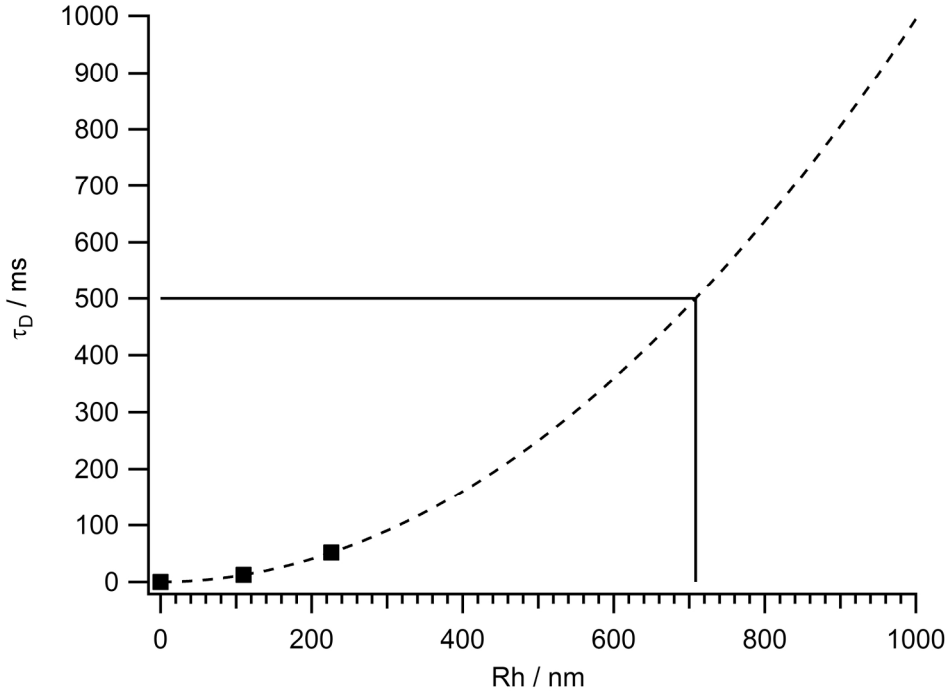

Figure 5. Estimation of the hydrodynamic radius Rh of the CNF. Two particle sizes with their diffusion time, plus the origo, were converted from Wu et al.63, adjusted for the viscosity of DMSO, and fitted with a second order polynomial for extrapolation.
95x69mm (600 x 600 DPI)

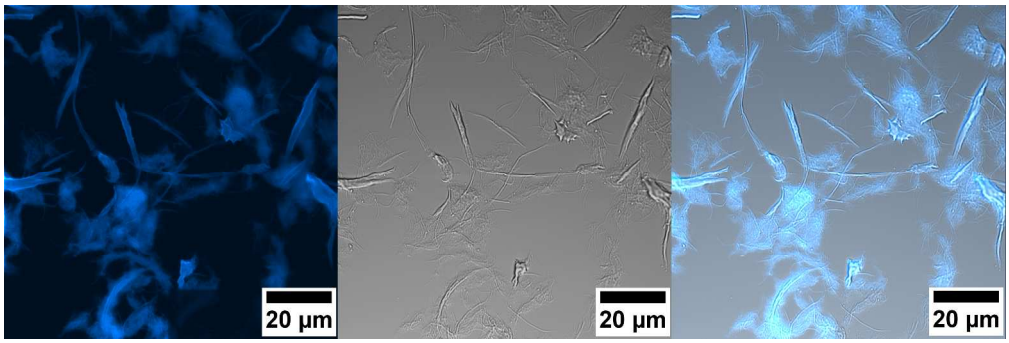

Figure 6. Confocal scanning laser microscopy imaging of LY labelled on the block copolymer-modified CNF. (Left) Fluorescence image obtained with an excitation wavelength of 405 nm, (middle) bright-field image (right) combined overlay fluorescence-bright-field images.
1498x499mm (72 x 72 DPI)

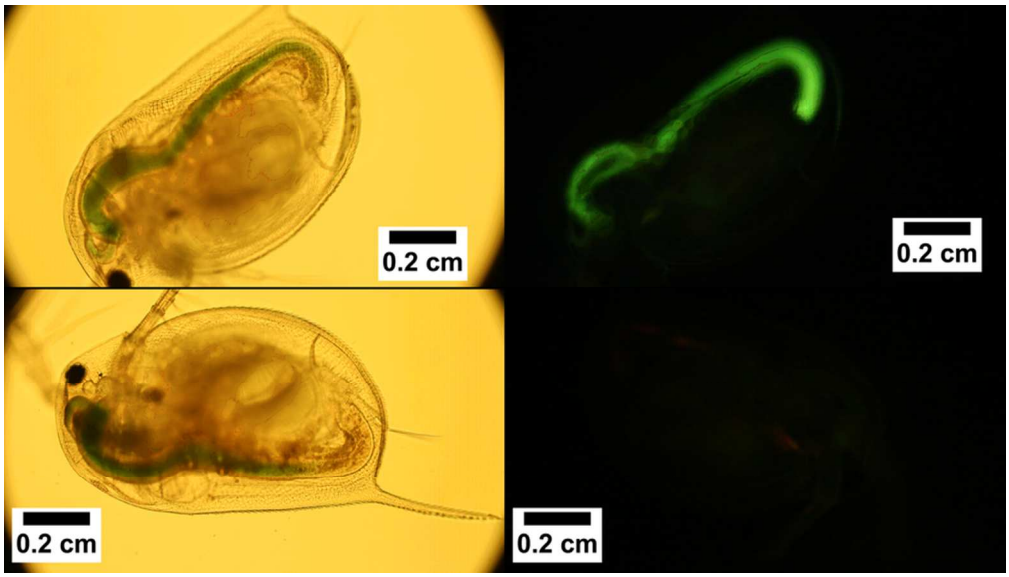

Figure 7. Bright field (left) and fluorescence (right) images of Daphnia magna in (bottom) control experiment and (top) exposed to LY-CNF.
352x199mm (72 x 72 DPI)